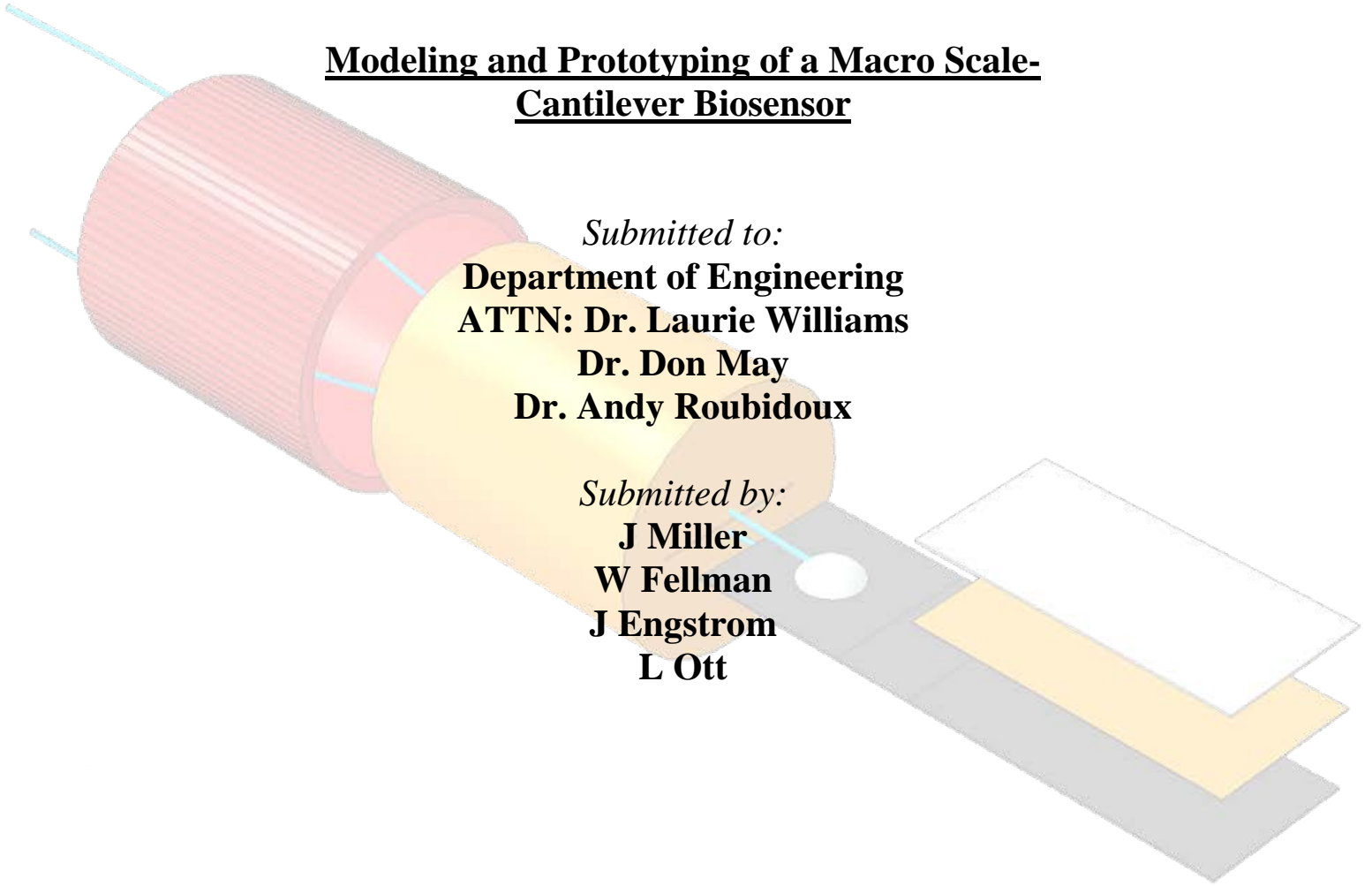


FORT LEWIS COLLEGE

Modeling and Prototyping of a Macro Scale-Cantilever Biosensor



Submitted to:

**Department of Engineering
ATTN: Dr. Laurie Williams
Dr. Don May
Dr. Andy Roubidoux**

Submitted by:

**J Miller
W Fellman
J Engstrom
L Ott**

ABSTRACT

Development of potable water systems throughout the less developed world necessitates a rapid and accurate method of water quality analysis. Poor water quality is commonly determined by the presence of *E. coli*. This bacterium leads to multiple health problems and in the cases of the elderly or very young ingestion of *E. coli* may lead to death. Currently a device known as a biosensor is under development. This device utilizes change in the natural frequency to detect small masses such as *E. coli* and requires much less time in comparison to current methodology. Although there are multiple types of biosensors the most sensitive to small changes in mass is the dynamic piezo-electric millimeter size cantilever, or PEMC. This project investigates the mass sensitivity and construction of a dynamic PEMC. Due to the difficulties associated with construction, prototype cantilevers are scaled to the centimeter scale. To reduce the number of prototypes constructed, computer models are developed and validated to within 12% of published values. This model is then utilized to predict response of prototype cantilevers. To analyze sensitivity to mass change a series of experiments are performed measuring the change in frequency with the addition of 10 μg , 20 μg , and 30 μg respectively. The prototype cantilevers performed as expected showing significant shifts in frequency due to mass with the best equipment resolution being in the range of 2 to 3 kHz with a mass sensitivity of 130 Hz/1 μg .

INTRODUCTION

BACKGROUND

Contamination of drinking water sources by Escherichia coli (E. coli) is a major cause of mortality in developing parts of the world, and is also a concern in the USA. Currently the EPA considers a water source to be contaminated with any tests being positive for E. coli. American cities test reservoirs for E. coli multiple times throughout the day to account for any fluctuation with water surge. The EPA allows only 5.0% of these samples to test positive and all positive tests are retested (EPA).

A single E. coli weighs 1 picogram, which is too small to be 'weighed' conventionally. Detection must be accomplished through mechanical or chemical means. Chemical testing is expensive because testing strips and chemical additives are replaced after each test. The use of chemical testing has a number of drawbacks such as the expense of testing strips, the strips and chemicals are single use, a longer testing period of 24-48 hours, and the human error associated with results analysis. Besides lacking resources, the dynamic nature of some rural peoples' water supply is such that frequent testing is warranted to guard against sudden outbreaks. A quick and easy drinking water test for coliforms would help to suppress E. coli outbreaks around the world.

Biosensors are a quick and easy mechanical alternative for E. coli detection. The most common type of biosensors is a composite cantilever beam consisting of a glass and piezoelectric layer. The glass layer is chemically treated with a process known as silanization, which allows it to capture bacteria from the fluid medium. In comparison to the chemical strips utilized in an incubator, the treated section of a PEMC may be utilized multiple times requiring only a cleaning between samples.

Mass detection is achieved through static or dynamic operation. Static sensors detect transient forces from the binding of an incident mass. Dynamic cantilevers are forced to vibrate while the natural frequencies are monitored for changes induced by mass attachments. Previous research by Mutharasan and Johnson has established the increased sensitivity of dynamic mode cantilevers. This project will investigate the sensitivity of dynamic type cantilever biosensors.

The development of a piezoelectric cantilever biosensor is a promising breakthrough for recognizing bacteria within a sample. Research has been done on these biosensors, but their effectiveness has not been perfected. These biosensors have potential to be fast, portable and effective biosensors.

GOAL AND OBJECTIVES

The goal is to construct piezo-electric cantilevers and quantify mass sensitivity.

Primary objectives:

- Construct finite element model of previously published cantilever
- Refine the finite element model by comparing frequency values to published data within 5%
- Construct prototypes of a centimeter scale cantilever.
- Measure frequency response in the cantilever with no mass added
- Measure frequency response in the cantilever with known added mass
- Maintain a minimum of 95% repeatability within the prototype population

- Correlate frequency response shift to known added mass

PROBLEM DEFINITION AND SCOPE

This objective of this project is to model and construct piezoelectric excited cantilevers (PECs). These will be used to quantify the sensitivity due to mass change. Such detection is useful for determining if a new water source is potable as well as if an existing source has been contaminated.

A piezoelectric excited cantilever is a complex device. The material utilized to induce vibration in the cantilever is known as lead zirconate titanate (PZT) this material is a manmade ceramic that acts as an electromechanical coupled device. When an electric potential is placed across the PZT a deformation results, due to the attachment point of the cantilever this deformation results in vibration of the cantilever. The resonant frequency of the bare cantilever is determined by measuring the minimum phase shift—the cycle shift between the driving signal and the feedback, or output signal—across a wide range of frequency inputs. Once determined, the resonant frequency of the bare cantilever provides a reference datum for the cantilever-PZT system behavior. Because the resonant frequency is unique to the geometry and material properties of the cantilever as *E. coli* cells attach to the cantilever the mass is increased. The change in mass affects results in a shift of the resonant frequency. Using this process the relative mass-concentration of the pathogen in the water can be determined (Campbell).

The size of the cantilever arm dictates the sensitivity of the device. This is due to the fact that the smaller the cantilever, the greater the ratio of pathogen to cantilever mass (Campbell). Disadvantages of smaller cantilevers include limited surface area for antibodies and reduced durability. Objectives for the computer model are to predict sensitive modes by analyzing frequency shift due to added mass without having to repeatedly build prototypes.

The project encompasses optimizing sensor dimensions and devising accurate, repeatable manufacturing processes. Then empirical trials of the sensor are conducted by varying single-parameters in batch-runs of prototype units in order to establish a baseline for performance and modifications to our final design.

LITERATURE REVIEW

BIOSENSORS

Theory for this project originates in chapter 18 of Zourab ET AL and the Ph.D. thesis of Gosset A Campbell (Campbell and Mutharasan). Both pieces of literature provide general insight into cantilever physics. Equations relating modal geometry (Equations 3 and 4), eigenfrequency and mass sensitivity (Equation 5) are presented on pages 464-466 of Zourob ET AL. To better understand the derivations it is necessary to examine the work of John Sader (1998).

Computer models for this project are based on work by Blake Johnson (2011). Johnson is a Ph.D. candidate at Drexel University. Of all articles examined, his had the most detailed description of a computer model. However, the information provided is insufficient for duplication of the computer model. Despite the lack of material, data in Johnson's paper is still valuable as a computer modeling goal.

The article from Johnson and Mutharasan (2012) is useful for visualizing modal geometries and understanding how cantilever theory has changed since the publication of Campbell's thesis. One section outlines the superior sensitivity of dynamic over static mode sensors. It explains why cantilevers of millimeter scale are more useful in water than those of the micro scale. It outlines the latest theory behind mass sensitivity, and lists application dependent optimization parameters for cantilevers.

A paper by Ashton Poole, of Fort Lewis College provided an introduction to the material as well as the experimental basis for this project to expand upon. Poole outlined the need for E. coli sensors in 3rd world countries, and demonstrated acceptable sensitivity of a PEMC for E. coli detection. This project improves on his work through investigation of accurate cantilever fabrication, computer aided design, and enhanced extraction and analysis of sensitivity data.

THEORY AND DESIGN OPTIONS

FUNCTION

Cantilevers achieve sensation through the static or dynamic modes of operation. Static cantilever sensors have a piezoelectric layer (PZT) that sends a signal when it bends. Static sensors bend when a small mass binds to them; this produces a transient electric signal notifying observers of the mass.

Dynamic mode cantilevers also have a PZT layer; user controlled forces excite the PZT to induce vibration. An oscilloscope or similar device is used to monitor vibration and compute the resonance frequency of the cantilever. Mass attachment is evident upon observation of a frequency change. Extremely small masses cause observable changes in natural frequency of the beam. Dynamic sensors are the primary focus of this study because superior sensitivity has been established for this type (Johnson 2012).

Dynamic cantilevers may be excited and monitored through any combination of internal or external means. One method of external excitation is by tapping the cantilever with another piezoelectric device whereas internal excitation occurs when an electric signal is applied across the PZT. External monitoring may consist of a laser reflected from the cantilever surface to an observation point, or observation of acoustic waves. Internal monitoring is observing a signal from the vibrating PZT (Johnson, 2012). This project utilizes internal excitation and monitoring.

Cantilever design depends on user requirements and four optimization parameters. Varying applications require cantilevers with different (1) mass sensitivity, and (2) dynamic range. Optimization must also account for (3) the viscosity of measuring environment (gas or fluid), and (4) the acceptable time frame for detection to be achieved (Johnson). The four optimization parameters are discussed below with relation to user needs.

Parameter 1: Mass sensitivity

A live E. coli cell has a mass of 1 picogram. The EPA has zero tolerance for E. coli in drinking water. Therefore water quality testers require picogram sensitivity. Current experimental values for sensitivity range from 10 to 50 hz (Johnson, 2011).

High order modes and lightweight cantilevers have maximum mass sensitivity. The magnitude of the mode is limited by the sensitivity of frequency extraction equipment. High modes are difficult to observe because they have smaller displacement amplitude. The effective mass must be minimized, but not at the expense of parameter 2 (Sader).

Parameter 2: Dynamic range

Dynamic range describes cantilever ability to detect masses both large and small. A cantilever with large dynamic range can sense any mass from femtograms up to milligrams. High order modes (above 20Khz for PEMCs) are good for detecting on the order of femtograms. Higher modes are unsuitable for detecting large masses because the frequency shift is so high that the peak may be rendered indistinguishable from

neighboring modes. Lower modes are suitable for detecting large masses because they experience smaller frequency shifts and will not be confused with neighboring modes. Wide dynamic range is achieved through monitoring high and low order modes (Johnson 2012).

Parameter 3: Viscosity of surrounding fluid

Viscosity of the fluid medium (μ) surrounding the cantilever dictates optimum cantilever size. If the cantilever dimensions are too small viscous forces dominate the system. Viscous forces are undesirable because they damp out the cantilever resonance spectrum. Cantilevers, of micron scale, are only suitable for dynamic operation in low viscosity environments such as air (Zourab et al). Water testing cantilevers need larger dimensions to overcome viscous damping forces and have observable modes.

Equation 1 is Reynolds number R_e for a cantilever vibrating in fluid. To limit the influence of viscous forces the flow regime across the cantilever must be turbulent. Reynolds number depends on cantilever width, height, length, b , h and L respectively. Vibration frequency also effects R_e . Each frequency is associated with eigenvalues α , indicating that R_e is large when vibration is fast. To achieve turbulent flow cantilever dimensions must be adjusted such that the Reynolds number is greater than 2300 for the desired eigenvalue α .

$$R_e = \frac{\alpha^2 \rho_w h b^2 \sqrt{hE}}{4\mu L^2 \sqrt{3(4\rho_c h + \pi\rho_w b)}} \quad (1)$$

Reynolds number also depends on density ρ_c and elastic modulus E of the cantilever and density of surrounding environment ρ_w . See appendix A for the derivation of Eqn. 1

Parameter 4: time frame for detection

Detection time frame is how quickly the mass of interest bonds to the cantilever. Random drifting of E. coli cells suspended in a fluid sample determines detection speed. Increasing cantilever surface area and sample concentration increases the chance for a Brownian encounter, resulting in faster detection. Detection may also be accelerated by inducing sample circulation, increasing cantilever size, or constructing an array of cantilevers.

Results from past experimenters indicate that a 1x5mm cantilever responds to 50 to 100 E. coli cells per milliliter in a 10 minute time frame (Zourab et al). This time frame is acceptable for water quality testing. In fact, it is 144 times faster than most chemical tests.

METHODOLOGY

MODAL FREQUENCY AND GEOMETRY EXTRACTION

Finite element analysis (FEA) is performed in a program called Abaqus CAE. The two models shown in figure 1 are analyzed, one duplicates a millimeter sized cantilever (PEMC) from peer reviewed literature (Johnson 2011), and the other models centimeter sized prototypes (LPECs). Copying Johnson’s computer model serves to validate the process of model construction. Once the modeling process is validated, we can confidently predict behaviors of cantilever prototypes. FEA predicts better sensitivity for cantilevers with high elastic modulus and for nodes experiencing large displacement.

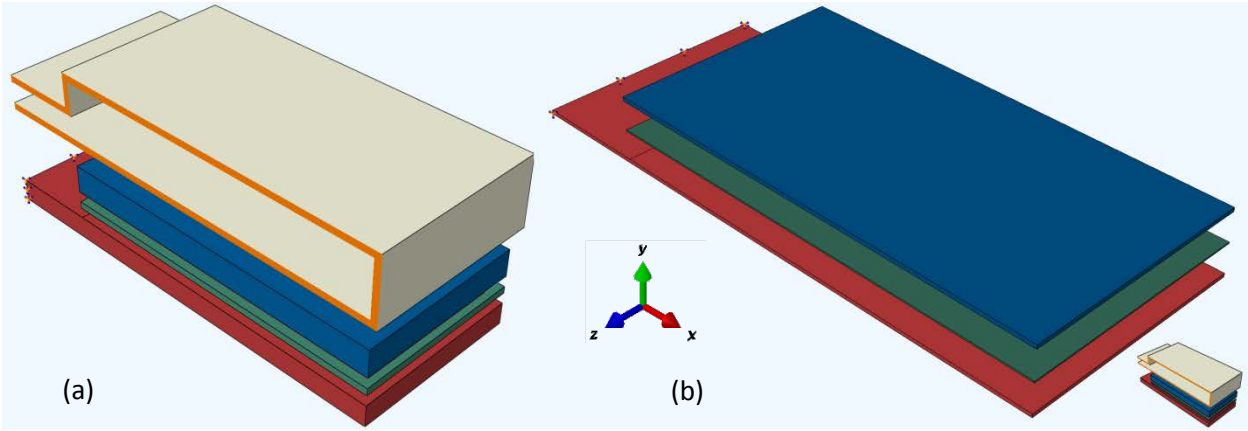


Figure 1: Exploded views of PEMC(a) and LPEC (b) models. The PEMC is shown to scale beneath the LPEC. The orange surface is a cross section cut through a 40micron polyurethane layer. Red layers are PZT, blue is silica, and green layers are cyanoacrylate adhesive. Anchor constraints indicated by nodes on the right of each cantilever.

First, each layer is drawn separately, and material properties assigned to each. All layers require definitions for mass, elastic modulus and poisons ratio (Table 1). Transverse grain orientation must be assigned to the PZT layer because it has an anisotropic elastic modulus. All other layers have homogenous material properties.

Table 1: Below are all inputs for both computer models from figure 1. Lead zirconate titanate (PZT) is not modeled with Poisson's ratio of Youngs Modulus. Instead an elastic stress tensor (Table 2) is used to simulate the anisotropic behaviors of this material.

Material Data	color code	PEMC dimensions (mm)	LPEC dimensions (mm)	density (kg/m ³)	Poisson's	Youngs modulus (Pa)
Silica	blue	0.16 X 2 X 1	Not used	2200	0.17	73.1x10 ⁹
Cyanoacrylate	green	4x10 ⁻⁵ X 2 X 1	4x10 ⁻⁵ X 20 X 10	1100	0.35	17.0x10 ⁸
Polyurethane	white	4x10 ⁻⁵ thickness	Not used	1000	0.33	1.0x10 ⁸
Borosilicate Glass	blue	Not used	0.16 X 20 X 10	2400	0.2	62.8x10 ⁹
PZT	red	0.127 X 2.5 X 1	0.127 X 25 X 10	7750	NA	NA

Table 2: The anisotropic elasticity tensors for Piezo Systems® PZT 5a and 5h are shown below. PZT 5a is specified for the PEMC. PZT 5h is used in construction of LPEC prototypes and the model.

$$E_{PZT5A} \begin{Bmatrix} C_{11} & C_{12} & C_{13} & 0 & 0 & 0 \\ C_{21} & C_{22} & C_{23} & 0 & 0 & 0 \\ C_{31} & C_{32} & C_{33} & 0 & 0 & 0 \\ 0 & 0 & 0 & C_{44} & 0 & 0 \\ 0 & 0 & 0 & 0 & C_{55} & 0 \\ 0 & 0 & 0 & 0 & 0 & C_{66} \end{Bmatrix} = \begin{Bmatrix} 12 & 7.52 & 7.51 & 0 & 0 & 0 \\ 7.52 & 12 & 7.51 & 0 & 0 & 0 \\ 7.51 & 7.51 & 11.1 & 0 & 0 & 0 \\ 0 & 0 & 0 & 2.11 & 0 & 0 \\ 0 & 0 & 0 & 0 & 2.11 & 0 \\ 0 & 0 & 0 & 0 & 0 & 2.26 \end{Bmatrix} \cdot 10^{10} \frac{N}{m^2} \quad \text{Johnson 20112011}$$

$$E_{PZT5H} \begin{Bmatrix} C_{11} & C_{12} & C_{13} & 0 & 0 & 0 \\ C_{21} & C_{22} & C_{23} & 0 & 0 & 0 \\ C_{31} & C_{32} & C_{33} & 0 & 0 & 0 \\ 0 & 0 & 0 & C_{44} & 0 & 0 \\ 0 & 0 & 0 & 0 & C_{55} & 0 \\ 0 & 0 & 0 & 0 & 0 & C_{66} \end{Bmatrix} = \begin{Bmatrix} 18.5 & 13.7 & 9.7 & 0 & 0 & 0 \\ 13.4 & 18.5 & 9.7 & 0 & 0 & 0 \\ 9.7 & 9.7 & 14.8 & 0 & 0 & 0 \\ 0 & 0 & 0 & 6.2 & 0 & 0 \\ 0 & 0 & 0 & 0 & 6.2 & 0 \\ 0 & 0 & 0 & 0 & 0 & 2.6 \end{Bmatrix} \cdot 10^{10} \frac{N}{m^2} \quad \text{Piezo Systems}$$

The technique best matching the literature (Johnson 2011) includes drawing each layer separately and applying tie constraint interactions to adjacent surfaces. Polyurethane and cyanoacrylate surfaces contacting PZT and glass are defined as slave surfaces, while corresponding surfaces on the PZT and silica are defined as master surfaces. The FEA program requires these definitions to determine which surface penetrates the other during deformation. Slave materials are assigned tetrahedral 3d stress elements and mesh is applied over a network of seeds spaced 0.06mm apart. Master materials (PZT and silica) must have larger elements than slaves materials, so they are meshed over 0.12mm seeds. Quadratic interpolation and nonlinear geometry calculation options are activated.

The natural frequencies and vibration shapes of cantilever beams are found using Euler Bernoulli beam theory. Equation 2 is a 4th order partial differential equation for transverse displacement y as a function of longitudinal distance x and time t . The first term accounts for spring force within the beam and depends on material elasticity E and cross sectional inertia I . The second term accounts for inertial forces of the vibrating beam and depends on cantilever density ρ and cross sectional area hb . The final term of the equation accounts for damping forces characterized by a damping constant c_o .

$$EI \frac{\partial^4 y}{\partial x^4} + (\rho hb) \frac{\partial^2 y}{\partial t^2} + (c_o) \frac{\partial y}{\partial t} = 0 \quad (2)$$

To solve the finite element model, separation of variables is used to create a weak form of equation 2. A computer vectorizes the weak form as shown in equation 3 where M and K are mass and stiffness matrices and ω is a matrix containing natural frequencies. Another function relates the eigenvector ξ to the ω is a matrix. Lanczos eigensolving then reveals the secrets of equation 3 (Dassault Systèmes).

$$(-\omega^2 M^{MN} + K^{MN}) \xi^N = 0 \quad (3)$$

Lanczos eigensolving is an efficient simplification of Arnoldi iteration. It's primarily used to solve large scale matrix equations. It requires relatively few large scale matrix operations because mass and stiffness are defined as hermitian matrices (Arbenz). Abaqus CAE can also extract natural frequencies using AMS and subspace iteration methods, but Lanczos is required for computation of effective mass (Dassault Systèmes).

FEA modeling does not use equations 3 and 4 to find modal geometry. Instead it derives participation factors by substituting results from equation 3 into equation 4 (Dassault Systèmes). Participation factors Γ_{ai} indicate the strength of motion for each node i and mode numbers α . Participation factors depend on the magnitude of rigid body response T_i at each node and the cantilevers effective mass m_α at each mode. Mode shapes are seen (figure 2) when the participation factors are plotted in 3d space.

$$\Gamma_{ai} = \frac{\xi_\alpha M T_i}{m_\alpha} \quad (4)$$

Observation of modal geometries provides clues about which modes have potential for sensing incident masses such as E. coli. The five main geometry types are shown in Figure. 2.

Internal and external forces on the cantilever influence the frequencies at which resonant modes occur. Internal forces are always the same for a given mode because the elasticity of the cantilever is constant. When a small mass such as E. coli attaches to the cantilever it exerts inertial forces as it oscillates with the cantilever. If the inertial forces of the attached mass are great enough relative to internal cantilever forces, the shift in resonant frequency will be observable, and thus the presence of the E. coli is known.

The first mode type is transverse (up and down motion) these modes are the most common because the cantilever is narrowest in this direction and easier to bend. Transverse modes have the greatest mass sensitivity because they have the least amount of internal force.

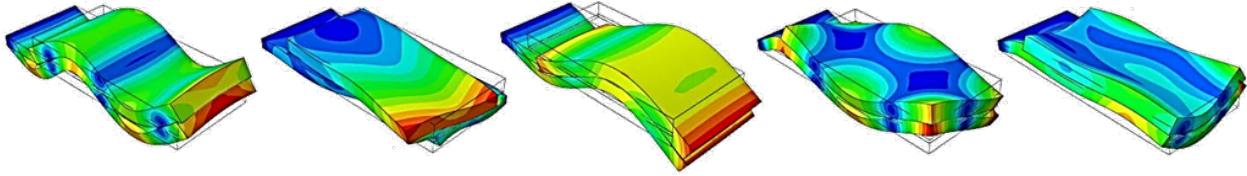


Figure 2.- Each shape above represents one of five main modal geometries predicted by Abaqus. These include; transverse, lateral, longitudinal, torsional, and buckling

Cantilever sensitivity is governed by Equation 6 (Zourab). It indicates largest sensation for small cantilevers and high order modes. Large frequency shift Δf given a small change in mass Δm enables detection of small mass. Small sensors increase this ratio because effective mass m_a is less and natural frequencies f_n are high. Effective mass is low for high order modes because many nodes on the surface don't move at all. When E. coli attaches to one of the few spots that is moving, its mass is greater with respect to the moving portion of the beam, giving it greater influence on the natural frequency.

$$\frac{\Delta f}{\Delta m} = A \cdot \frac{f_n}{2m_a} \quad (5)$$

The amplification factor A results from impedance change in the piezoelectric layer during resonance. A must be experimentally determined because it has no mathematic expression. To rectify their calculations previous observers have determined A values on the order of 10^8 for modes near 9kHz.

It must be noted that the driving impulse of the piezoelectric layer is purely longitudinal and transverse. Despite this the cantilever will resonate in transverse, longitudinal and buckling modes only because the driving impulse is the expansion and contraction of the PZT. This driving impulse cannot impart torsional or lateral vibration. The cantilever could resonate torsionally or transversely given the proper impulse, but that is not the kind of impulse used in this situation. The model data must be used selectively depending on geometry.

The sensitivity of piezoelectric cantilevers is largely dependent on size, and therefore also mass. Using computer models, the effects of scaling these cantilevers is observed. PEMCs achieve mass sensitivity on a picogram level, which cannot be achieved with centimeter sized cantilevers. The highest observable mode and amplification factor (Equation 6) for LPECs must be experimentally determined. The material available for the building of the prototypes is limited to one thickness, so thickness scaling could not be applied to the models. The polyurethane layer is also ignored for this observation.

A computer model is programmed for every scaling factor from the original PEMC model from 1 to 10. These models are used to determine the modal frequencies with and without a mass applied to the sensor. This mass is applied as a point mass at a specific node on the surface of the cantilever. The difference between these determined frequencies concludes a measurement of sensitivity.

From prototype testing, the seventh transverse mode is the most sensitive measurable resonance mode. The computer model states that there are more sensitive modes; however, those modes are not detected in the built prototype. For the largest scaled model (same dimensions as the built cantilevers), the seventh transverse mode results in a frequency shift of 26.9 Hz per microgram. The original PEMC model results in a frequency shift of 34200 Hz per microgram in this seventh transverse mode. The computer model results prove that if the prototypes created in this project are scaled to the original design parameters, the

sensor would be 1270 times more sensitive in measuring frequency shift. With the parameters given, the PEMC model would have a frequency shift of one hertz with the attachment of 30 E coli cells.

Due to material masses and internal damping, the properties can also affect the sensitivity. Although the lead zirconate titanate (PZT) and the silica properties cannot be altered, there are several options of adhesives for application on the cantilever. Using the finite element analysis models, the properties that permit the maximum sensitivity can be determined. Cyanoacrylate, epoxy, and a material with a high modulus of elasticity are analyzed for optimization of frequency shift.

The results proved that adhesives with higher modulus of elasticity are the most effective. When applied to the LPEC computer model, the maximum shift is 1180 Hz with the Epoxy and 1153 Hz with the cyanoacrylate. Although the properties of these adhesives affect the performance of the cantilevers, the manufacturing of the sensors once more influences the project. The cantilevers using epoxy as the adhesive are the most effective with the construction capabilities. An adhesive with higher elasticity would give us more frequency shift, but not by much. Although further research is encouraged, the increase in frequency shift sensitivity is minimal in comparison to dimensional alterations.

MODEL COMPARISON

To validate the output frequency response of the finite element model, the data is compared to a computer model published in a 2011 issue of *Sensors and Actuators B*. The article is titled The Origin of Low-order and High-order Impedance-coupled Resonant Modes in Piezoelectric-excited Millimeter-sized Cantilever (PEMC) Sensors: Experiments and Finite Element Models. This paper utilizes industry standard FEA software called COMSOL Multiphysics®.

Despite meeting industry standards, even the published model is not perfect. Figure 3 compares the COMSOL model with a professionally constructed prototype. Unexpected irregularities in professionally built PEMCs are enough to produce unexpected results. Misalignment of cantilever layers often results in extra torsional and asymmetric modes. These asymmetries cannot be accurately measured for incorporation into a computer model (Johnson 2011).

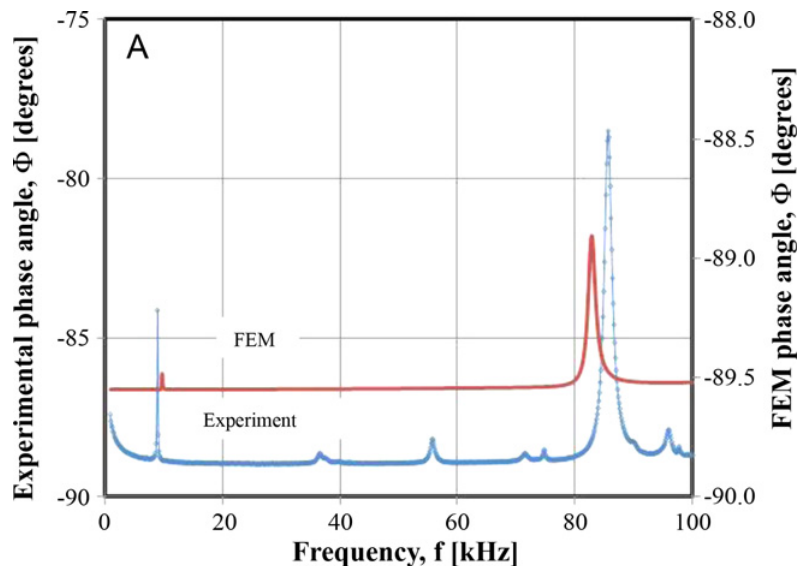


Figure 3.- Even Johnson's computer model (upper line) is not a perfect predictor of cantilever resonance (lower line). Minor asymmetry in his lab prototypes resulted in extra torsional modes. Computer models are good for getting a general feeling for PEMC behavior, but not an accurate picture of reality.

Modeling errors from false inputs are magnified with computational complexity. The lowest cantilever modes have the large displacements (computationally complex), but the simplest geometries. High order modes have complex geometries but small displacement. This implies that low order mode computations are more likely to predict inaccurate frequencies, and high order mode computations are likely to output faulty geometries. Modes that are neither high, nor low (10-20) are susceptible to compounding of both geometric and frequency miscalculations.

The computer model for this project and Johnson's trend similarly. Figure 4 shows natural frequencies within 10% of Johnson's computer model, the exception for middle modes (13, 14 and 15). The finite element model agrees with data from Campbell's research to within 15% (see Figure 4). By adjusting parameters in the finite element model it can be shown that the middle modes are most sensitive to user inputs such as mesh density, element types, and cantilever dimensions. The middle modes are most sensitive because they are more geometrically complex than lower modes and have larger displacements than higher modes.

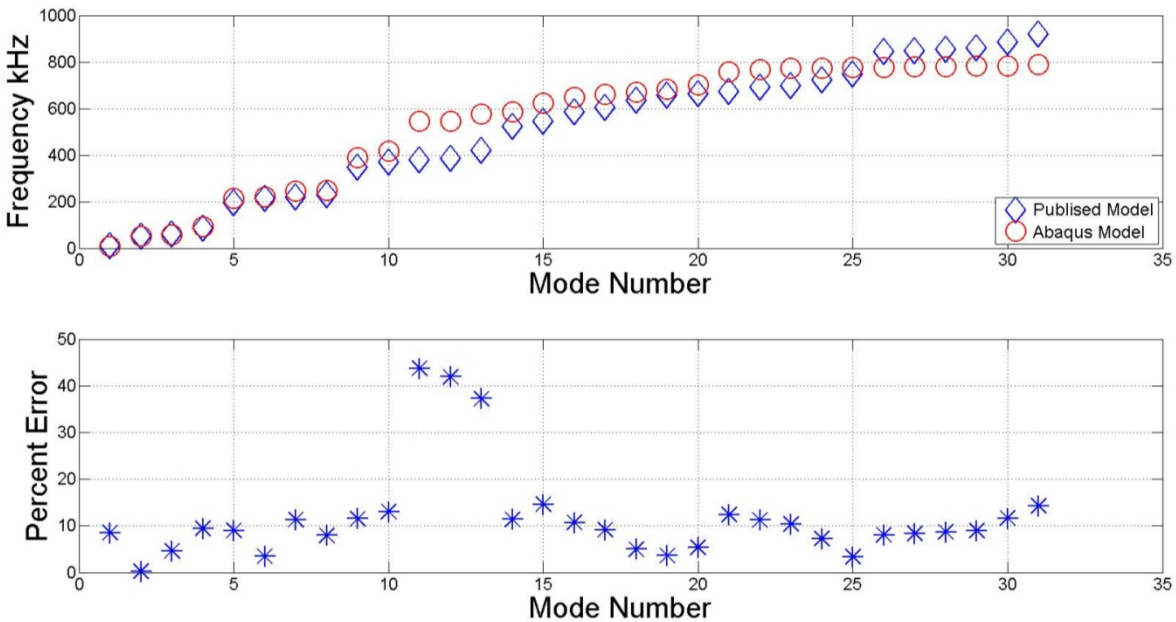


Figure 4.- This is the spectrum of resonance modes predicted in FEA models. The Abaqus model used in this project has an average deviation of 11.8% from Johnson's published model. A portion of this difference can be accounted for in that Campbell's model accounts for structural damping, while this option is not implemented Abaqus. Modes 11-13 seemed the most sensitive to changes in mesh size and layer interaction definitions.

Difficulties in reproducing Johnson's model arise from lack of information, and incomplete knowledge of the software utilized to create the finite element model. His article does not specify mechanical properties for the bonding layer, nor does it state dimensions for the polyurethane coating. Some of this data was acquired through e-mail communication. Due to the value of this computer model for future patents it is possible that its author is intentionally tight lipped on the subject. Other modeling uncertainties arise when choosing what type of interaction to specify between the layers. The use of inter-layer tie constraints yields results closest to Johnson's model.

It must be taken into account that no computer model will result in perfect data but can serve as a valid approximation to cantilever response. In order to validate new models as well as to gain design knowledge of functional cantilevers further lab testing is required.

LAB DATA AND COMPUTER MODEL COMPARISON

To enhance the correlation between lab data and FEA computations, an intricate computer model is employed. This model includes the anchoring medium and accounts for clamping forces on the housing. This better approximation comes with higher computational expense, job run times exceeding 1 hour. The intricate model consumes too much time for design optimization purposes (where only the cantilever end is modeled), but is a better approximation of reality.

To match the computer model with experimental results FEM geometry must be examined. Figure 5 shows how FEM calculates all possible modes of vibration, but lab data is only a small set of electrically observable modes. As a result there are many FEM modes that don't correspond to any lab data. Some FEM modes most closely matching the lab data must be discarded because they feature geometries where the PZT is stationary and cannot produce electric signal. Many FEM modes that do exhibit PZT resonance don't manifest themselves in lab experiments because they are masked by destructive interference and random noise.

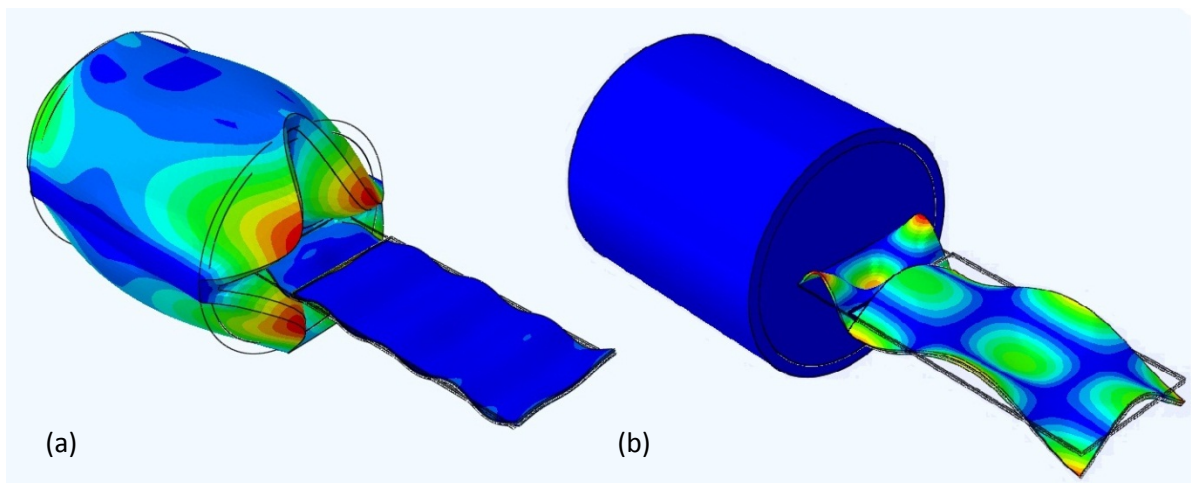


Figure 5.- A non PZT mode (a) and a PZT mode (b). The non-PZT modes are not electrically observable because the PZT does not move enough to generate a signal. FEM analysis predicts all modes of vibration. Many of these modes do not correlate to data gathered in the lab. When matching FEM modes to lab data it is important not to pick unobservable modes.

The vibration spectra of physical prototypes and the LPEC computer model are shown in figure 6. Physical prototype frequencies match the computer model within 2%. This correlation is better than for the PEMC model comparison (Figure 4). The superior correlation results from better knowledge of the LPEC components than for those of the PEMC. Errors in the programming methods for the LPEC model are less prevalent because cantilever vibration is more symmetric at the centimeter scale than it is at the millimeter scale. Thanks to symmetry, the LPEC computer model is less complex resulting in less propagation of programming errors.

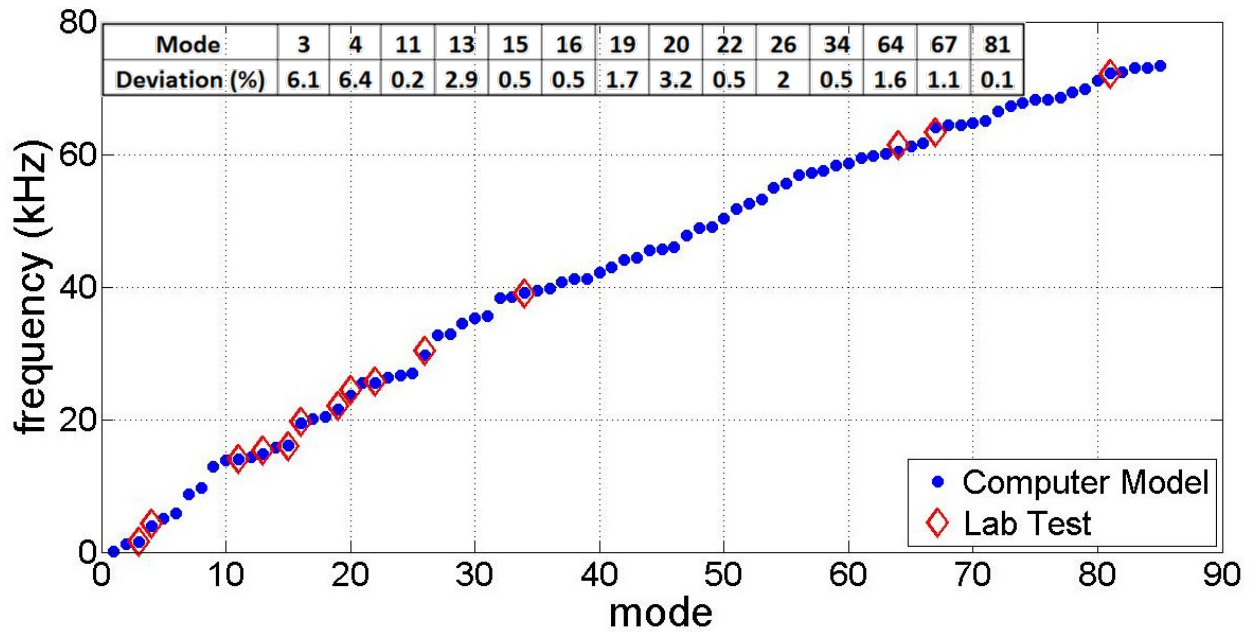


Figure 6.-Frequency data gathered in the lab matches the unloaded LPEC model within 2% on average. However, not all modes predicted by the model are electrically observable. Many modes do not have enough PZT displacement to generate electric signal (fig. 5). Destructive signal interference also renders many modes unobservable.

CONSTRUCTION METHODS

Construction methods are executed such that prototypes exhibit identical resonance frequency and mass sensitivity. Repeatability depends on producing cantilevers with consistent dimensions. The construction process is fine-tuned to avoid breaking the prototypes.

All components of a LPEC are shown in figure 7. The PZT is 10x35x0.127mm, glass and bonding layers measure 10x20mm and have 0.14 and 65 micron thickness respectively. The anchoring medium encapsulates the rear 10mm portion of the PZT, copper leads, and solder joints. The anchor is 16.8mm in diameter and 20mm long. The housing has an outer diameter of 18.6mm.

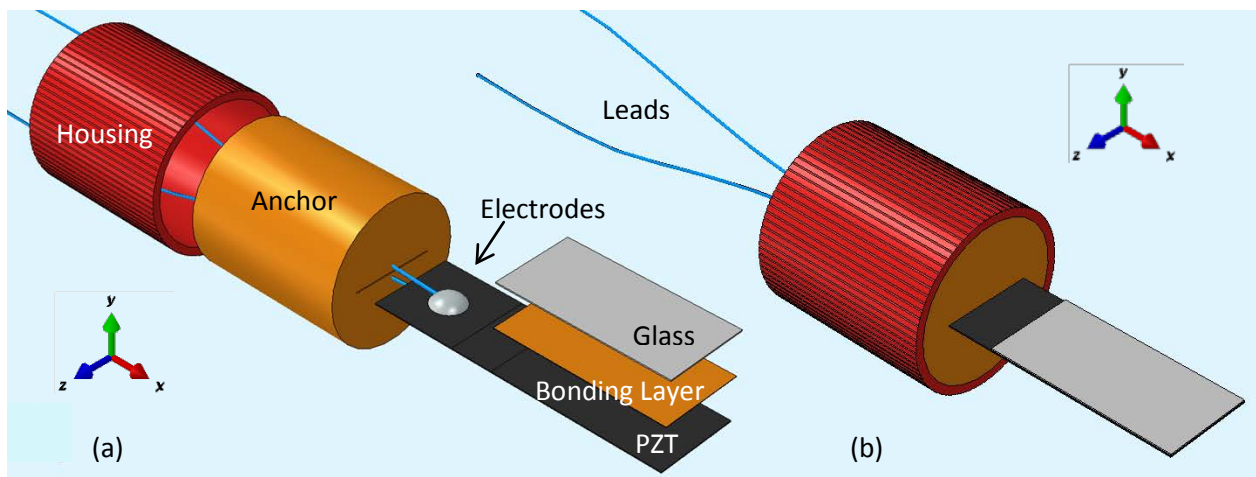


Figure 7. - An exploded view (a) and complete assembly (b). The blade consists of piezo systems® PZT 5H and no. 1 microscope slides. The anchor and bonding layer are epoxy and housing consists of fire formed plastic.

Cantilever construction involves 6 basic steps:

- 1) Cut PZT, glass, and housing to appropriate dimensions (Figure 7)
- 2) Solder leads to the rear of the PZT
- 3) Secure PZT and housing on a casting surface (Figure 8)
- 4) Cast the anchoring medium
- 5) Remove casting device
- 6) Apply bonding layer between glass and PZT (Figure 9)

Step 1- To cleave glass and PZT a razor blade and straight edge are used to score along the line of desired separation. The tip of the razor exerts immense pressure upon the glass or PZT surface and forms a series of micro-fractures aligned with the stroke direction (Klimek). To avoid introducing extra fractures the cut must be performed on a smooth surface such as marble or plexiglass. The piece is sufficiently scored when a faint line becomes visible on its surface. The piece is then positioned on the edge of a block and tapped causing a clean break along the line of stress fractures.

Step 2- Silver solder, Harvey's solder paste, and copper wires between 0.15 and 0.4mm diameter are used. Soldering temperatures between 240 and 300°C are recommended (Morgan Tech). First, solder paste is applied to the leads and PZT surface. Then solder is applied, maximum application time is 2 seconds, any longer and the sputtered nickel electrodes of the PZT surface will disintegrate. Lastly the flux must be cleaned off with a paintbrush and gasoline or acetone. Wires greater than .35 mm in diameter are not recommended, once they are soldered on the force required to bend them will break the PZT.

Step 3-The anchoring medium (epoxy) is always formed within the housing, but an additional surface is necessary to stop it from flowing onto other portions of the cantilever. This casting surface is what forms the forward anchor face; it should be perpendicular to the cantilever and as planar as possible. Two equally precise methods (Figure 8) for creating this surface may be used.

The first casting method is to stick the PZT into a leveled tube of lard (Figure 8b). The housing is positioned atop the lard and epoxy poured in the top. Care must be taken not to insert the PZT too deeply or off vertical, a guide is necessary. PZT insertion and extraction should not be attempted if the lard is below 21C.

The second method is to use casting blocks (Figure 8a). One block has a slot milled into its surface, the other is flat. The PZT is sandwiched between the two, and then the housing and epoxy are applied in a similar manner as in the lard method. Prior to PZT insertion grease must be smeared on the inner block surfaces to stop epoxy from running down the crack. Highly viscous (axle) grease is used, thinner grease wicks up the protruding PZT during casting, thereby compromising the anchor. To prevent cohesion a sheet of packaging tape is stuck to the block tops and smeared with a thin layer of grease. The upper block surface is marked to ensure consistent housing placement.

The housing must fit inside protective cover to protect the cantilever during transportation. The standard housing is a 20mm fire formed section of 16ga shot shell. This fits perfectly into a 12ga (19mm) shell encapsulating the cantilever for protection during transportation. To precisely cut the housing, an extra-long section is slipped onto a mandrel, and cut to 20mm on a lathe.



Figure 8. - Two methods to form the anchoring medium, casting blocks (a) and lard surface (b). Epoxy is poured into a housing that rests upon either of these horizontal surfaces. Care is taken to ensure a level casting surface that resists bonding with the anchoring medium. Any type of housing may be used in conjunction with the casting surface. Consistency in housing dimensions is recommended.

Step 4-The anchoring medium is 3 parts West Systems 105 epoxy resin and one part West Systems 207 hardener. This slow curing epoxy is preferred over 5 minute epoxy, because bubbles have time to evacuate. The presence of bubbles in 5 minute epoxy compromises the consistency of the anchoring surface. The heat generated by 5 minute epoxy makes it unsuitable for lard casting.

Step 5-Success in removing cantilevers from their cast requires that they not stick. In the case of lard, the temperature must be 21C before insertion or removal of the PZT. If the lard is below 70°F excessive cohesion breaks the PZT. When using casting blocks, successful removal depends on complete grease coverage. The grease must be highly viscous to avoid wicking up onto the electrode end of the cantilever. Incomplete grease coverage results in the PZT bonding to the casting blocks, making successful removal unlikely.

Step 6-The best bonding layer investigated in this project consists of West Systems epoxy. Initially cyanoacrylate was used. Due to rapid curing the cyanoacrylate hardened before it spread over the intended surface and before the glass was properly aligned (see Figure 9). To create a 65micron layer, 13 microliters of adhesive is oozed with a micropipette. The adhesive must be applied along the centerline to avoid forming bubbles when it spreads.

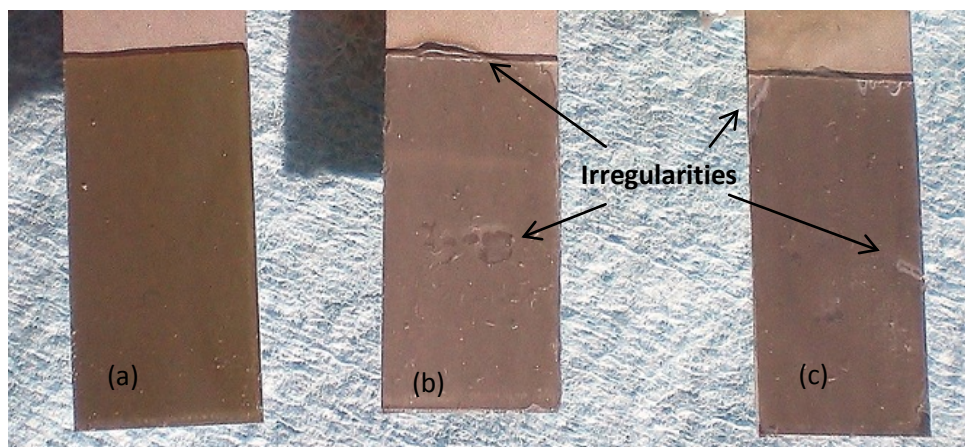


Figure 9.-Bonding layers. Note the irregularities in the cyanoacrylate bonded cantilevers (b and c). Long cure time of the epoxy (a) allows time for capillary action to spread the bonding layer evenly between the glass and PZT surfaces. Epoxy is also favored because its rigidity causes less damping of inertial forces from incident mass, thus increasing sensitivity.

PERFORMANCE TESTING AND ANALYSIS

DATA ACQUISITION

To find the RF spectra experimentally, the piezo-sensor is first connected as shown in Figure 8, then excited with a driving signal and allowed to respond naturally. In essence, the sensor is simply “pinged” and then allowed to ring just like a bell, in tune to its natural frequencies. As the pitches change due to mass added to the sensor, this change in frequency can be measured.

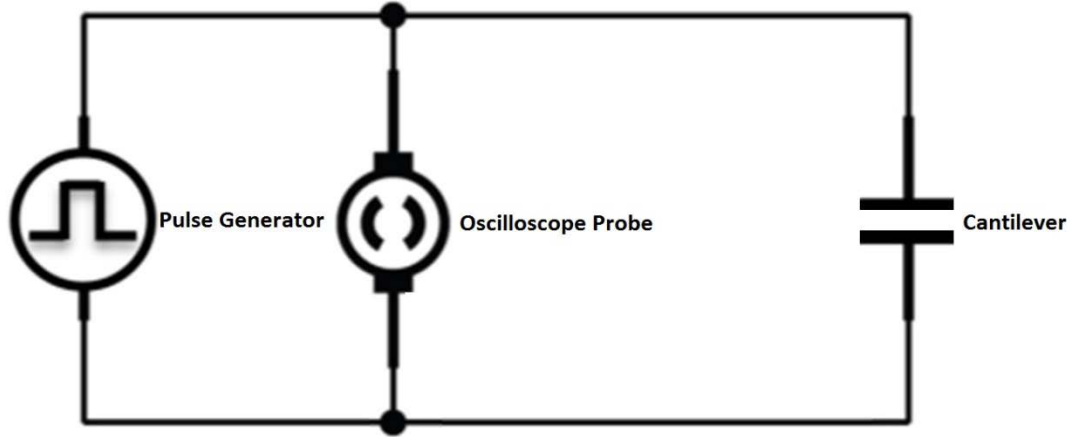


Figure 10: Circuit diagram of experimental setup

This method is a departure from prior experiments of this nature and is an attempt to improve the process with sights on possible future automation. Interface with the sensor has previously been achieved by sweeping a sine-wave of linearly varying period through a range of frequencies and measuring impedance of the sensor itself as a function of this driving frequency (Poole)(Campbell). While effective, this requires considerable time, computation power, and additional instrumentation that could be rendered obsolete by more straight-forward methods. Harmonic analysis has now been employed in an effort to minimize the processing requirements on future revisions to this sensor. This greatly simplifies the process and will aid future automation efforts.

Rather than continuously driving the sensor through a varying range of frequencies and measuring two disparate signals simultaneously, the system employed here excites the sensor with a single pulse function allowing the sensor to react naturally in tune to its inherent resonant modes. In this manner a single input channel can be monitored and recorded for data analysis and no driving signal is required during actual acquisition, thereby also eliminating any chance of error associated with the driving signal itself.

The pulse signal used to excite the sensor is produced by a Tektronix AFG 3021B programmable waveform generator and is intended to approximate a Dirac delta function. The Dirac delta function, δ , is the approximation of an infinitely large voltage spike over an infinitely short period of time normalized to 1. It can also be considered as a Gaussian distribution as that distribution tends to zero and can be expressed as follows in equation 6 where variable a represents the width of the pulse and x is the independent variable.

$$\delta_a(x) = \frac{1}{a\sqrt{\pi}} e^{-x^2/a^2} \quad (6)$$

In the analysis of the lab test data the primary tool used is the Discrete Fourier series analysis function in Matlab vector mathematics computation software. As can be shown from equation 7, any function $f(x)$

can be approximated by the Fourier transform of the function $F(t)$ as a series of ordered sine waves (shown here as Eulerian equivalent ordered complex exponentials.)

$$F(t) = \sum_{n=1}^N x(n) \omega_N^{(n-1)(t-1)} \quad (7)$$

$$x(n) = \left(\frac{1}{N}\right) \sum_{t=1}^N F(t) \omega_N^{-(n-1)(t-1)} \quad (8)$$

$$\omega_N = e^{-j(2\pi)/N}$$

Where $F(t)$ is the Fourier transform (FFT), x the independent variable, t represents time, n is an integer counter, and N is the limit of the range of interest. Similarly it must follow by Equation 9, where k is the period of the time-domain transform that as the width of the driving pulse grows infinitely narrow that there are infinite variations of sine waves that must comprise that function. Hence the sensor is able to be stimulated with a burst of frequencies spanning the entire range of interest in a single brief instant allowing the operator to then sample those particular frequencies which resonate within the sensor.

$$F_x[\delta(x - x_0)](k) = \int_{-\infty}^{\infty} e^{-2\pi i k x} [\delta(x - x_0)] dx = e^{-2\pi i k x_0} \quad (9)$$

In order to sample the resonant frequencies, the LPEC is connected to a single channel of a Tektronix TDS 2012B digital data-logging oscilloscope set to communicate directly to a computer via Tektronix logging software.

The waveform response of the cantilever sensor is recorded in time domain through the connection, (Figure 11) then the leading 200 data points are discarded to account for inevitable ringing in the system that occurs due to the nature of the driving impulse.

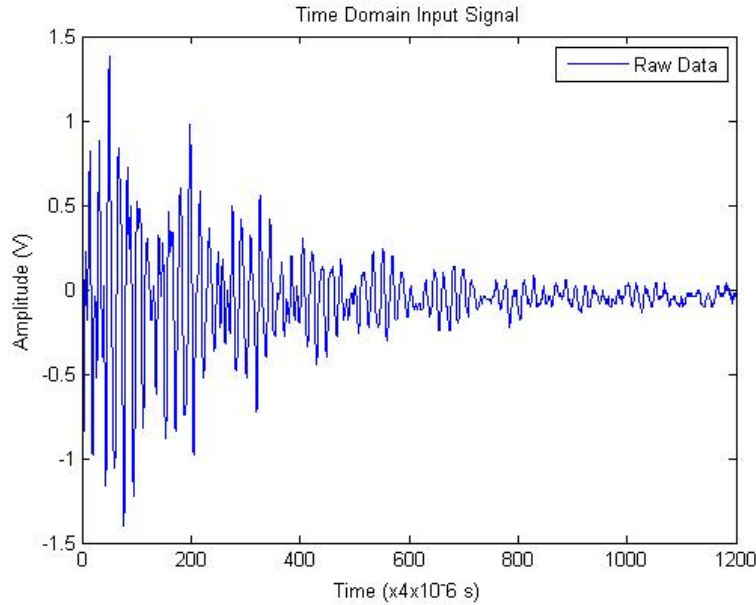


Figure 11: Response of the cantilever in the time domain. This signal is recorded with an oscilloscope.

This signal is then decomposed based on the FFT model in order to identify the resonant frequencies of all modes simultaneously as shown in Figure 12.

DATA ANALYSIS AND RESULTS

The spectra now decomposed into their frequency components are then plotted (Figure 12) and the components identified via Matlab GUI functions. This is currently the ‘bottleneck’ in this acquisition process and should be improved upon by automating a function to output a table of modal frequencies.

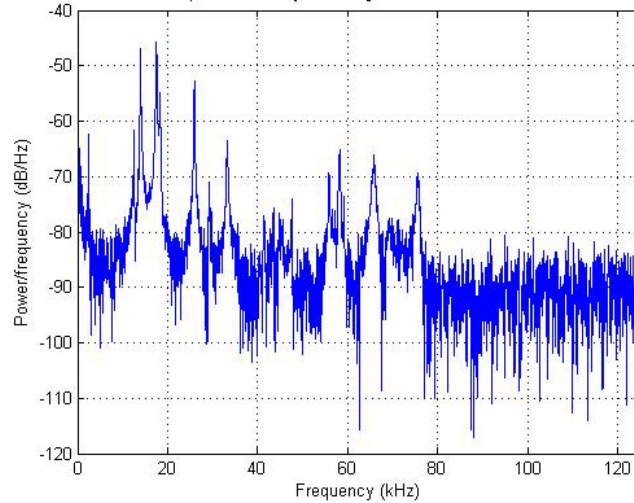


Figure 12: Direct Fourier Transform model of data. The peaks indicate what frequencies have the strongest amplitude. These are the natural/resonance frequencies.

In testing mass sensitivity, mass is applied to the cantilevers via a graduated pipette in 10 μ l increments to 30 μ l and the corresponding resonant mode frequencies recorded. Based on sampled data a phase shift of the responding resonant modal frequencies can be observed (Figure 13).

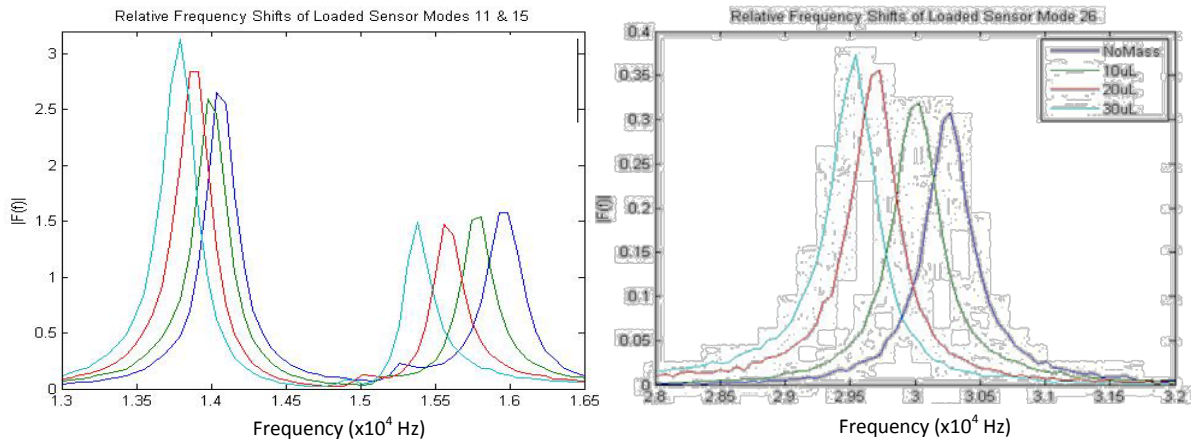


Figure 13: Modes 11, 15, and 26 respond to 10 μ l water droplets with a phase shift. The frequency decreases after each addition of mass.

The relatively poor resolution of the frequency shift is attributed to the relatively long sampling period (0.1s) necessary to encompass sufficient cycles for acceptable resolution. With the oscilloscope capable of recording only a finite number of data points (2500) a compromise was made between high sampling frequency and duration of sample. The large size of the cantilevers results in being on the upper end of the capabilities of the equipment for capturing sufficient responses over a sufficient duration as shown in Figure 13. Smaller cantilevers operating at higher frequencies should not experience this limitation.

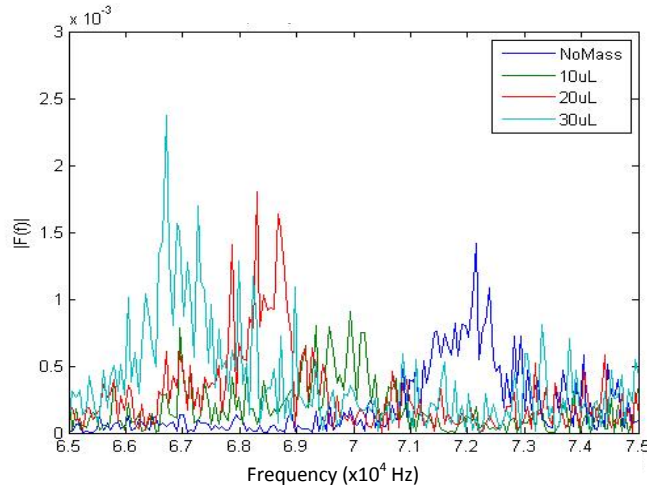


Figure 14: High modes such as the 81st shown here have excellent sensitivity but poor resolution. Better resolution may be obtained from an oscilloscope capable of collecting more than 2000 time points.

The resolution of measurements can immediately be significantly improved with existing equipment by employing an external triggering link between the pulse generator and the oscilloscope. This would allow the use of a 100MS/s (mega-sample per second) rate rather than the 250MS/s rate employed for this experiment. This would allow more than doubling of the data range leading to higher resolution in the frequency domain. The faster rate utilized in this experiment was necessary to properly time the internal triggering via the pulse on the input channel.

Preliminary testing indicates a region of greatest sensitivity for the large scale cantilever sensors to be within the 15th and 26^h modes of resonance, as can be seen in figure 13. A typical spectrum signature for this sensor is shown in figure 12. The sensitivity per added mass can be seen in figure 15. These correspond to an average phase shift of 130 ± 31 Hz per μL , or 130 ± 31 Hz/ μg for this sensor.

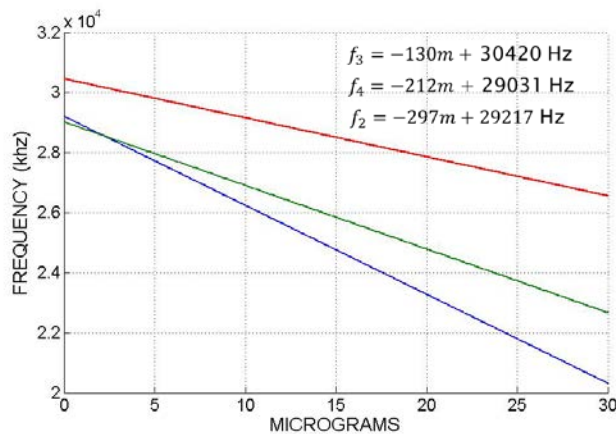


Figure 15: Phase-Shift relationships for mode 26 between sensors correlating to mass addition. Each line represents a different prototype.

As can be seen from the Gamma series of cantilevers, the un-calibrated un-weighted consistency is ± 250 Hz. This corresponds to manufacturing repeatability of the cantilevers sampled. Considering these are operating at an average frequency of 29,935 Hz for this mode, this places the gross manufacturing specs to within $\pm 1\%$. This is well within this projects targeted manufacturing repeatability of $\pm 5\%$.

The sensitivity of the response is altogether much poorer than expected. While the gross geometries were sufficiently large to allow for repeatability, there are fine inconsistencies which still cannot be adequately addressed without sufficiently precise manufacturing capabilities. These resulted in different relative sensitivities of each of the sensors on the order of $\pm 39\%$ over all sensors together. However, each individual sensor maintained a linear response to mass within $\pm 24\%$ over the range, bolstering the finding that the majority of this error is due to sampling rates as opposed to manufacturing anomalies.

CONCLUSION

LPECs are useful for biosensor simulation because their size is convenient for observation and fabrication. The biosensor prototype testing verifies a linear decrease in frequency due to added mass. For each 10 μ g of mass added to the sensor, the resonance of the 7th transverse mode decreased by approximately 2kHz. This gives the cantilever a sensitivity of roughly 200Hz per microgram. This is larger than computer model predictions for sensitivity at 26.9 Hz per microgram.

Although the computer model accurately determines resonance modes of the cantilevers, it is unable to calculate the frequency shifts due to added mass. Right now the FEA model is mainly useful for relative predictions and observing general trends. Previous researchers rectify modeling errors with an amplification factor.

To sense an E. coli cell, a biosensor is required to have a resonance shift of 1Hz per picogram. Computer modeling predicts that PEMCs are 1200 times more sensitive than the LPECs. With more development in modeling, construction, testing, and time, the use of a millimeter scale cantilever to detect E. coli is more than a conceptual idea.

Different bands of the frequency spectrum exhibit different qualities. The low frequency modes have minimal mass sensitivity. On the contrary, high frequency modes are more sensitive but exhibit poor resolution. To improve resolution an oscilloscope capable of sampling more than 2000 time points is required. The best balance of peak sensitivity and resolution for the tested cantilevers occurs at the 7th transverse mode near 30kHz.

CONTINUING RESEARCH

One of the difficulties confronted in this project was the corroboration of experimental data to computer model data. Computer modeling has suggested increased sensitivity on cantilever nodes experiencing large displacements. These predictions and direct relationships have yet to be verified experimentally.

Once the exact relationship between the cantilever model and prototypes can be determined, tests mapping the most sensitive locations can be compared to computer predictions. Then changes modeled can be used to more accurately predict the behavior of prototypes.

The large scale of LPEC prototypes is convenient for this purpose, as the placement of mass at specific locations is much simpler. However to succeed in detecting particles on the scale of E. coli, cantilever dimensions must be no larger than 1x5mm. Future cantilevers should be smaller scaled to increase their sensitivity.

Future experimenters are advised not focus as stringently on the repeatability of cantilever dimensions. Inconsistent fabrication may be remedied through individual sensor calibration. Other options include having a professional fabricator build prototypes for testing, or researching other biosensor requirements. Instead, the focus should be silanizing glass surfaces and the construction of a sample flow cell.

Appendix A

To find Reynolds number for a vibrating cantilever, equation A1 is substituted into A2 and all that into A3 (Sader 1998).

$$\omega_{\text{vac},1} = \frac{C_1^2}{L^2} \sqrt{\frac{EI}{\mu}} \quad (\text{A1})$$

$$\frac{\omega_{\text{fluid}}}{\omega_{\text{vac}}} = \left(1 + \frac{\pi \rho b}{4 \rho_c h} \right)^{-1/2} \quad (\text{A2})$$

$$\text{Re} = \frac{\rho \omega b^2}{4 \eta} \quad (\text{A3})$$

ω_{vac} is angular frequency in a vacuum (normal frequency f is obtained by dividing by 2π)

ω_{fluid} is angular frequency in fluid

μ is cantilever mass per unit length

η is viscosity

C is the eigenvalue associated with the mode of interest

b is cantilever width

h is cantilever thickness

ρ_c is density of the cantilever

ρ is density of the fluid environment

I is the moment of inertia of a beam cross section, given by $\frac{1}{12}bh^3$

Appendix B

Example Matlab Code for producing DFT analysis:

```
%%  
  
x0 = xlsread('g3nomass1.CSV', 1, 'E200:E2500')  
x1 = xlsread('g3_10ug1.CSV', 1, 'E200:E2500')  
x2 = xlsread('g3_20ug1.CSV', 1, 'E200:E2500')  
x3 = xlsread('g3_30ug1.CSV', 1, 'E200:E2500')  
  
%%  
  
%Modes Gamma3 -- No Mass  
  
fs = 250000; % Sample rate per second  
m = length(x0); % Window length  
n = pow2(nextpow2(m)); % Transform length  
y = fft(x0,n); % DFT of signal  
f = (0:n-1)*(fs/n); % Frequency range  
p0 = y.*conj(y)/n; % Power of the DFT  
  
%plot(p(1:700,1),'DisplayName','p(1:700,1)','YDataSource','p(1:700,1)');figure(gcf)  
plot(f,p0)  
axis([0,35000,0,4])  
xlabel('Frequency (Hz)')  
ylabel('|F(f)|')  
title('Component Frequencies Of Gamma3 Unloaded Prevalent Modes')  
  
%%  
  
%Modes Gamma3 -- No Mass  
  
fs = 250000; % Sample rate per second
```

```

m = length(x0); % Window length
n = pow2(nextpow2(m)); % Transform length
y = fft(x0,n); % DFT of signal
f = (0:n-1)*(fs/n); % Frequency range
p0 = y.*conj(y)/n; % Power of the DFT

%plot(p(1:700,1),'DisplayName','p(1:700,1)','YDataSource','p(1:700,1)');figure(gcf)
plot(f,p0)
axis([35000,100000,0,.003])
xlabel('Frequency (Hz)')
ylabel('|F(f)|')
title('Component Frequencies Of Gamma3 Unloaded Additional Modes')

%%
%Modes Gamma3 -- No Mass

fs = 250000; % Sample rate per second
m = length(x0); % Window length
n = pow2(nextpow2(m)); % Transform length
y = fft(x0,n); % DFT of signal
f = (0:n-1)*(fs/n); % Frequency range
p0 = y.*conj(y)/n; % Power of the DFT

%plot(p(1:700,1),'DisplayName','p(1:700,1)','YDataSource','p(1:700,1)');figure(gcf)
plot(f,p0)
axis([100000,200000,0,.003])
xlabel('Frequency (Hz)')
ylabel('|F(f)|')
title('Component Frequencies Of Gamma3 Unloaded Additional Modes')

```

```

%%
%Modes Gamma3 -- 10 uL Water Added

fs = 250000; % Sample rate per second
m = length(x1); % Window length
n = pow2(nextpow2(m)); % Transform length
y = fft(x1,n); % DFT of signal
f = (0:n-1)*(fs/n); % Frequency range
p1 = y.*conj(y)/n; % Power of the DFT

```

```

%%
%Modes Gamma3 -- 20 uL Water Added

```

```

fs = 250000; % Sample rate per second
m = length(x2); % Window length
n = pow2(nextpow2(m)); % Transform length
y = fft(x2,n); % DFT of signal
f = (0:n-1)*(fs/n); % Frequency range
p2 = y.*conj(y)/n; % Power of the DFT

```

```

%%
%Modes Gamma3 -- 30 uL Water Added

```

```

fs = 250000; % Sample rate per second
m = length(x3); % Window length
n = pow2(nextpow2(m)); % Transform length
y = fft(x3,n); % DFT of signal
f = (0:n-1)*(fs/n); % Frequency range

```

```
p3 = y.*conj(y)/n; % Power of the DFT
```

```
%%
```

```
%Modes Gamma3 -- No Masss Raw Spectral Density Periodogram
```

```
Hs=spectrum.periodogram;
```

```
psd(Hs,x0,'fs',fs)
```

```
title('Raw Spectral Density Periodogram for Gamma3 Unloaded')
```

```
%%
```

```
%Modes Gamma3 -- 10 uL Water Added Raw Spectral Density Periodogram
```

```
Hs=spectrum.periodogram;
```

```
psd(Hs,x1,'fs',fs)
```

```
title('Raw Spectral Density Periodogram for Gamma3 w/10uL Water Added')
```

```
%%
```

```
%Modes Gamma3 -- 20 uL Water Added Raw Spectral Density Periodogram
```

```
Hs=spectrum.periodogram;
```

```
psd(Hs,x2,'fs',fs)
```

```
title('Raw Spectral Density Periodogram for Gamma3 w/20uL Water Added')
```

```
%%
```

```
%Modes Gamma3 -- 30 uL Water Added Raw Spectral Density Periodogram
```

```
Hs=spectrum.periodogram;
```

```
psd(Hs,x3,'fs',fs)
```

```
title('Raw Spectral Density Periodogram for Gamma3 w/30uL Water Added')
```

%%

Gamma3PhaseMatrix = [p0,p1,p2,p3];

Gamma3Phase3Plot(Gamma3PhaseMatrix)

%%

Gamma3PhaseMatrix = [p0,p1,p2,p3];

Gamma3Phase4Plot(Gamma3PhaseMatrix)

%%

Gamma3PhaseMatrix = [p0,p1,p2,p3];

Gamma3Phase11Plot(Gamma3PhaseMatrix)

%%

Gamma3PhaseMatrix = [p0,p1,p2,p3];

Gamma3Phase16Plot(Gamma3PhaseMatrix)

%%

Gamma3PhaseMatrix = [p0,p1,p2,p3];

Gamma3Phase19Plot(Gamma3PhaseMatrix)

%%

Gamma3PhaseMatrix = [p0,p1,p2,p3];

Gamma3Phase22Plot(Gamma3PhaseMatrix)

%%

Gamma3PhaseMatrix = [p0,p1,p2,p3];

Gamma3Phase26Plot(Gamma3PhaseMatrix)

```

%%

Gamma3PhaseMatrix = [p0,p1,p2,p3];
Gamma3Phase81Plot(Gamma3PhaseMatrix)

With representative PhasePlot program:
function Gamma3Phase26Plot(Gamma3_Phase)
% Plots mode 26
%Gamma3PhaseEndPlot(Gamma3PhaseMatrix)
% Gamma3PhaseMatrix: matrix of y data

% Auto-generated by MATLAB on 06-Mar-2012 12:57:47

% Create figure
figure1 = figure;
% Create axes
Fs = 250000; % Sample rate per second
n=4096;
f = (0:n-1)*(Fs/n); % Frequency range
% axes1 = axes('Parent',figure1);
% box(axes1,'on');
% hold(axes1,'all');

% Create multiple lines using matrix input to plot
% plot1 = plot(Gamma3_Phase,'Parent',axes1);
plot1 = plot(f,Gamma3_Phase);
axis([28500 31000 0 .35]);
legend('NoMass','10uL','20uL','30uL')
xlabel('Frequency (kHz)')
ylabel('|F(f)|')
title('Relative Frequency Shifts of Loaded Sensor Mode 26')

```

```
set(plot1(1),'DisplayName','NoMass');  
set(plot1(2),'DisplayName','10uL');  
set(plot1(3),'DisplayName','20uL');  
set(plot1(4),'DisplayName','30uL');
```

Appendix C

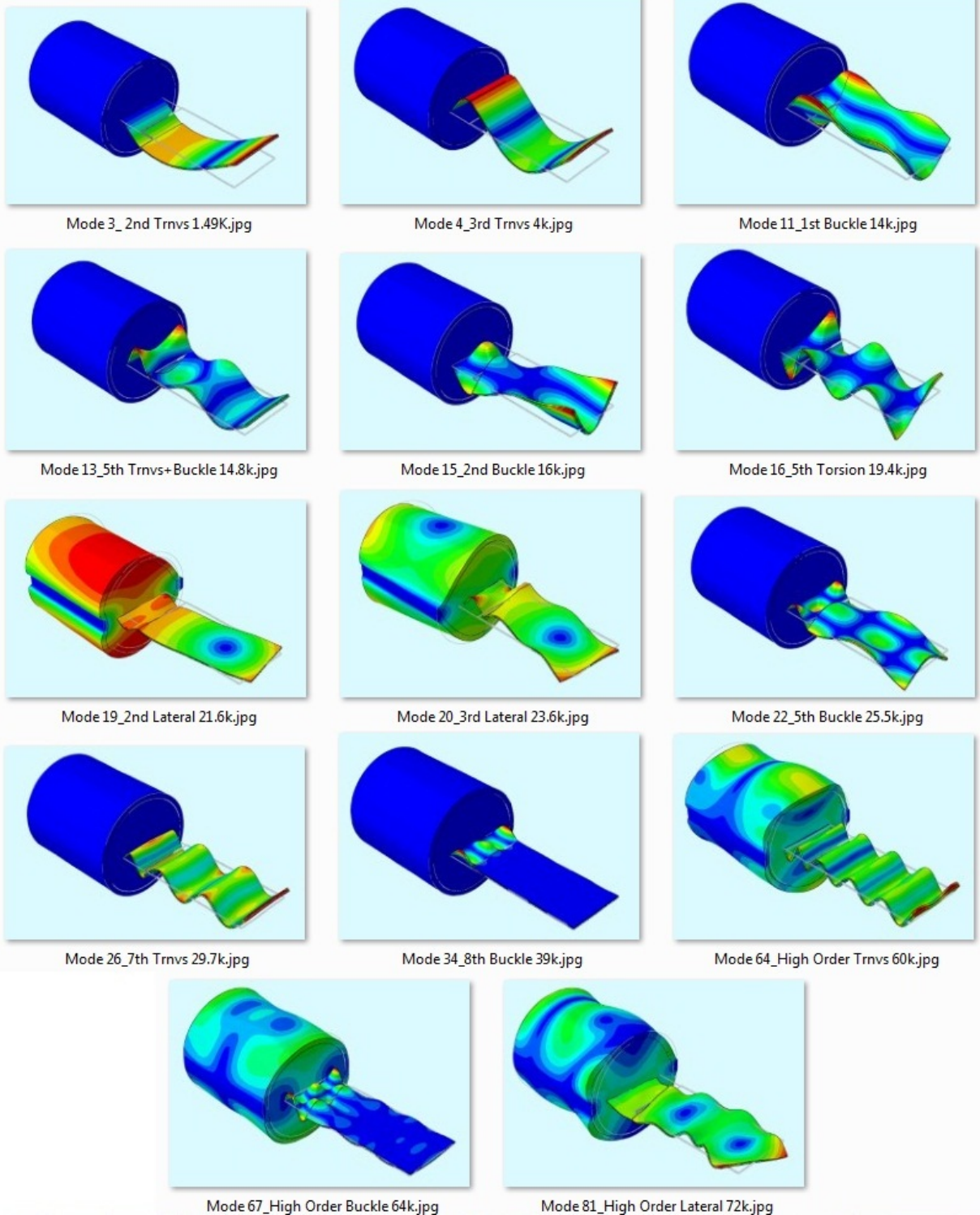


Figure A1-Above are exaggerated geometries for each natural frequency detected in the lab. The model predicts many natural frequencies, but only 14 are electrically observable. The peak associated with many of the modes is likely buried within signal ‘noise’ or canceled with destructive interference. Of the first 100 computer model modes only 14 were observed in the lab.

References

- Arbenz, Peter. "Lecture Notes on solving large scale eigenvalue problems: chapter 9 Arnoldi and Lanczos algorithms". <<http://people.inf.ethz.ch/arbenz/ewp/Lnotes/lsevp.pdf>>. Eidgenössische Technische Hochschule Zürich. accessed 2/14/12.
- Campbell, Gosset, A., Mutharasan, Raj. "Detection and Quantification of Pathogens, Proteins, and Molecules Using Piezoelectric-Excited Millimeter-Sized Cantilever (PEMC) Sensors." Drexel University (2006).
- Dassault Systèmes. *Abaqus 6.11 PDF documentation, Section 6.3.5-1 analysis users manual vol. 2.* [Vélizy-Villacoublay, France.](#)
- Dawkins Paul. *Paul's Online Notes.* Lamar University. <<http://tutorial.math.lamar.edu/Classes/LinAlg/Span.aspx>>. accessed 2/14/12.
- Environmental Protection Agency. *Drinking Water Contaminants.* <<http://water.epa.gov/drink/contaminants/index.cfm#4>>. Accessed 9-12-11.
- Habibi-Nazad, Bahram. *E-coli statistics.* <http://www.ccdb.ualberta.ca/CCDB/cgi-bin/STAT_NEW.cgi>. Accessed 9/14/11.
- Johnson, Blake N., Mutharasan, Raj. "Biosensing using dynamic-mode cantilever sensors: A review." *Biosensors and Bioelectronics* 32 (2012): 1-18. Electronic. (1)
- Johnson, Blake N., Mutharasan, Raj. "The Origin of Low-order and High-order Impedance-coupled Resonant Modes in Piezoelectric-excited Millimeter-sized Cantilever (PEMC) Sensors: Experiments and Finite Element Models." *Sensors and Actuators B: Chemical* 155.2 (2011): 868-77. Print. (2)
- Klimek Ralph.< <http://users.monash.edu.au/~ralphk/glass-cutting.html>>. Monash University, Melbourne 2007.

Morgan Technical Ceramics Co.

<<http://www.morganelectroceramics.com/products/piezoelectric/piezoelectric-electrodes/>>.
accessed 2/23/2012.

Mutharasan, Raj. "Curriculum Vitae,"

<http://www.chemeng.drexel.edu/faculty/individual/mutharasan/MutharasanCV%2008-01-08.pdf>

Poole, Ashton. *The testing and feasibility of piezoelectric excited millimeter sized cantilevers to detect pathogenic strains of Escherichia coli in third world water sources*. Fort Lewis College: April 23, 2010.

Romperé, A., Servais, P., Baudart, J., De-Roubin, M., Laurent, P. *Detection and enumeration of coliforms in drinking water: current methods and emerging approach*. Journal of Microbiological Methods 49 (2002) 31–54. Accepted September 10, 2001.

Sader, John Elie. "Frequency Response of Cantilever Beams Immersed in Viscous Fluids with Applications to the Atomic Force Microscope." Journal of Applied Physics 84.1 (1998): 64. Print

Zourob, M., Elwary, S., Turner, A. "Principles of bacterial Detection: Biosensors, Recognition Receptors and Microsystems." *SpringerScience+Business Media LLC* (2008): Print.